Evolution of microstructure, texture and topography during additional annealing of cube-textured Ni–5at.%W substrate for coated conductors

Wulff, Anders Christian; Mishin, Oleg; Grivel, Jean-Claude

Published in:
Journal of Alloys and Compounds

Publication date:
2012

Document Version
Publisher's PDF, also known as Version of record

Journal of Alloys and Compounds 539 (2012) 161–167

Contents lists available at SciVerse ScienceDirect

Journal of Alloys and Compounds

journal homepage: www.elsevier.com/locate/jalcom

Evolution of microstructure, texture and topography during additional annealing of cube-textured Ni–5at.%W substrate for coated conductors

A.C. Wulff [a,*], O.V. Mishin [b], J.-C. Grivel [a]

[a] Department of Energy Conversion, Technical University of Denmark, DK-4000 Roskilde, Denmark
[b] Section for Materials Science and Advanced Characterization, Department of Wind Energy, Technical University of Denmark, DK-4000 Roskilde, Denmark

ARTICLE INFO

Article history:
Received 14 March 2012
Received in revised form 4 June 2012
Accepted 6 June 2012
Available online 15 June 2012

Keywords:
Ni–W alloys
RABiTS
Annealing
Cube texture
Thermal grooving
Boundary migration

ABSTRACT

Microstructure, texture and topography have been studied in a recrystallized Ni–5at.%W substrate before and after additional annealing at 1025°C for 1 h. The initial recrystallized material contained a strong cube texture and a high fraction of low angle grain boundaries. Σ3 boundaries were also frequent in this substrate, including both coherent and incoherent twin boundary segments as well as non-twin Σ3 boundaries formed between twins and non-matrix neighbors of the cube texture component. A strong correlation between the boundary type and the average depth of grain boundary grooves was observed in this material. The smallest average groove depth was obtained for coherent twin boundaries, followed by low angle boundaries. Significantly greater average groove depths were found for the other boundary types. A similar correlation was also observed between the boundary type and the average inclination angle of groove walls. The additional annealing resulted in grain growth, texture strengthening and an increase in the fraction of low angle boundaries. Also, changes were observed in the extent of thermal grooving studied in the same regions before and after the additional annealing. Groove depths increased for a large number of stationary boundaries, whilst the majority of migrating boundaries developed shallower grooves compared to those before the additional annealing.

1. Introduction

Significant efforts have been made in the past two decades to increase the quality and efficiency of coated conductors, i.e. the second generation of high temperature superconducting tapes [1–8]. One method for manufacturing coated conductors utilizes a rolling assisted biaxially textured substrate (RABiTS) process to produce a strongly textured tape that is subsequently coated with a series of ceramic buffer layers and, finally, with a superconducting layer. In particular, this method has been applied for producing strongly textured Ni–W substrates coated with appropriate buffer layers and a superconducting $YBa_2Cu_3O_{7-\delta}$ (YBCO) layer [2–11]. The quality of such superconducting tapes greatly depends on the sharpness of the crystallographic texture, grain boundary (GB) misorientation distribution and surface conditions of the substrate material [2–13]. Since grain boundaries with misorientations greater than 10° dramatically decrease the critical current density of the epitaxially grown YBCO layer [7], the fraction of such boundaries in the substrate must be as low as possible. In the RABiTS process, the latter is achieved by annealing of a heavily rolled material to obtain a microstructure where most grains have orientations of the cube {001}⟨100⟩ texture. Surface roughness can be minimized either through the use of well polished rolls or by polishing of the substrate [12]. Excessive thermal grooving [14] should also be avoided by selecting appropriate heat-treatments.

It should be noted that the structural parameters and surface conditions of the annealed substrate may change during further processing. For example, crystallization of buffer layers [13,15] may be performed at higher temperatures than those used to anneal the substrate, which will likely increase the extent of GB grooving and may also modify the microstructure and texture of the substrate. These changes will inevitably affect characteristics of the buffer layer and, eventually, of the YBCO superconducting layer [8,13]. It is apparent that further optimization of the processing parameters for coated conductors requires an improved understanding of these changes.

In a previous communication we reported our preliminary results describing topographic changes in a recrystallized Ni–5at.%W substrate during additional annealing simulating conditions of a buffer layer crystallization process [16]. In the present work, these changes are considered in more detail, including analysis of groove depths for stationary and migrating boundaries. Also, the effect of the additional annealing on the boundary population and texture of the Ni–5at.%W substrate is characterized. A number of different techniques including atomic force microscopy

* Corresponding author.
E-mail address: anwu@dtu.dk (A.C. Wulff).

0925-8388/$ - see front matter © 2012 Elsevier B.V. All rights reserved.
http://dx.doi.org/10.1016/j.jallcom.2012.06.033

Fig. 1. Schematics defining the depth d and inclination angles β of the groove.

(AFM), scanning electron microscopy (SEM) and electron backscatter diffraction (EBSD) are applied to monitor changes in the same regions before and after additional annealing.

2. Experimental

2.1. Material

A Ni–5at.%W ingot was prepared by arc melting of 99.99% pure metals. The ingot was homogenized at 1025 °C for 87 h and hot forged into a rectangular shape with dimensions $8 \times 12 \times 97\ mm^3$, applying 0.5 mm thickness reduction per stroke. Following this hot deformation, the surface was polished mechanically to remove the oxide layer. The material was then cold rolled using mirror-finished rolls and applying less than 5% reduction per pass to a final thickness of 120 μm (98% total reduction). The sample was annealed in a protective atmosphere of 5% H_2 in N_2 at 1000 °C for 2 h. This annealed condition is referred in the present work to as condition A1. The sample was then additionally annealed in the protective atmosphere at 1025 °C for 1 h (condition A2). This temperature is within the range of that frequently used for buffer layer crystallization [13,15–18]. It is pertinent to mention that no evidence of secondary recrystallization was found in the given sample even when additional annealing was conducted at 1100 °C for 1 h. Vickers microhardness was measured in the annealed samples using a load of 200 g with a 15 s dwell time.

2.2. SEM/EBSD analysis

A field emission gun scanning electron microscope Zeiss Supra 35 was used for taking SEM images and for EBSD measurements (HKL Technology, Channel 5). Crystallographic texture was measured using the EBSD technique with a step size of 10 μm and covering an area of at least 5 mm^2 in the rolling plane. The fraction of the cube texture component was determined considering orientations within 10° from the ideal {001}⟨100⟩ orientation. A step size of 1–2 μm was applied for collecting smaller maps used for measuring grain size and GB misorientations. Because of the limited angular resolution of the EBSD technique, misorientations less than 1.5° were ignored in the EBSD maps. A misorientation threshold of 10° was used in the present work to distinguish between low angle grain boundaries (LAGBs) that do not dramatically affect the critical current density in the YBCO layer and high angle boundaries that substantially decrease it [7].

2.3. AFM analysis

Based on the features observed in the EBSD maps and corresponding SEM images, several regions containing different boundary types were selected for AFM analysis. The surface topography was characterized in these regions in contact mode using a Nanosurf easyScan 2 system, scanning over more than 17,000 μm^2 with a step size of 0.2 μm. Artifacts resulting from the AFM scanner exceeding its linear regime were treated using the standard data correction [19]. GB grooves were included in the roughness analysis and the arithmetic surface roughness was used to characterize the mean roughness. Following the approach described in Ref. [20], the groove depth d was measured as the distance from the groove root to the top of the groove wall (see Fig. 1). For asymmetric grooves, for which the heights of two walls were different, d was measured at the higher wall. To obtain a value characterizing the depth of an individual groove, the data were averaged over several AFM line scans across each groove. In addition, inclination angles β at the groove root (see Fig. 1) were determined from the AFM data and it was typically found that β_1 and β_2 were not identical.

3. Results

3.1. Annealed condition A1

The A1 condition contained a strong cube texture (see Fig. 2), where the area fraction of the cube component f_{cube} within 10° from the ideal {001}⟨100⟩ orientation was 96% (see Table 1). Most of the remaining area was occupied by grains with slightly greater deviations from the ideal cube orientation and by {212}⟨122⟩ twins in the cube-oriented matrix (Fig. 2). The microstructure was fully recrystallized with an average grain size of 25 μm (including annealing twins) and contained a high fraction of LAGBs, see Fig. 3. The fraction of boundaries with misorientations $\theta < 10°$ in the EBSD maps was 68%.z

The total fraction of Σ3 boundaries was measured to be 14%. This figure comprises true twin boundaries and non-twin Σ3 boundaries formed between annealing twins and non-matrix neighbors with orientations similar to that of the matrix grain (Fig. 4). Previous misorientation measurements in copper have shown that true twin boundaries are always characterized by small ($\Delta\theta < 3°$) deviations from the exact 60° ⟨111⟩ misorientation [21,22], whereas a wide range of deviations allowable by Brandon's criterion [23] are obtained for Σ3 boundaries between {212}⟨122⟩ twins and non-matrix cube-oriented neighbors [22]. Therefore, in

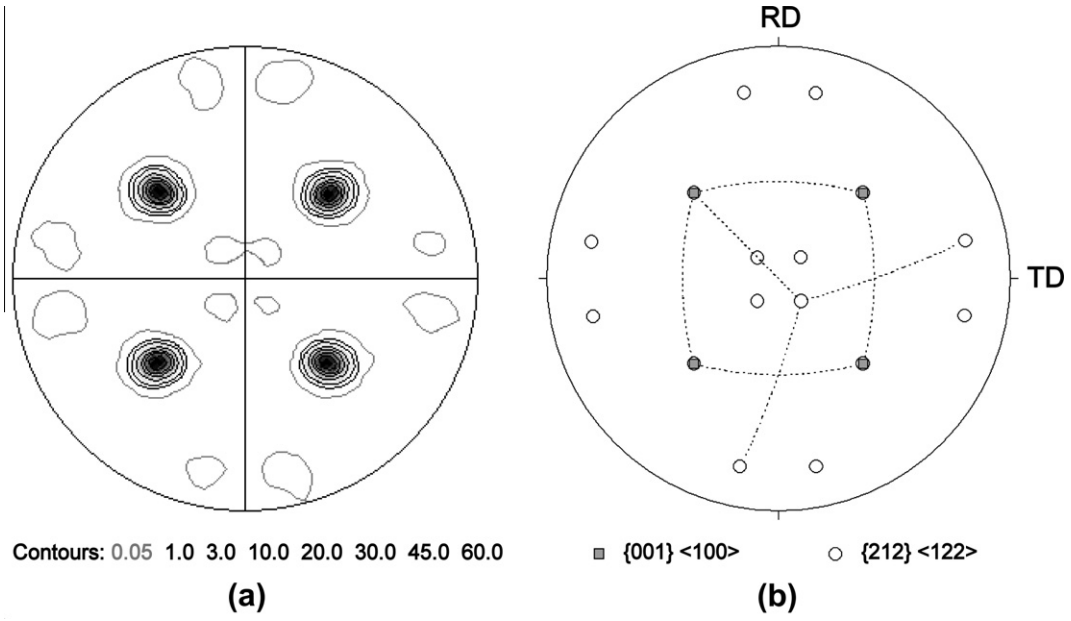

Fig. 2. Texture in the A1 condition: (a) {111} pole figure, (b) positions of the ideal {001}⟨100⟩ and {212}⟨122⟩ orientations [22]. Note the low intensity (gray contour) of the {212}⟨122⟩ orientations in (a).

Table 1
Parameters describing the microstructure, texture, surface roughness (S_A) and hardness (HV) of the Ni–5at.%W substrate in conditions A1 and A2.

Condition	Grain size (μm)	f_{cube} (%)	Fraction of boundaries (%)				$L_{A\ (\theta > 10°)}$ (μm^{-1})	S_A (nm)	HV
			$\theta < 10°$	$\theta > 10°$ except Σ3	Σ3 $\Delta\theta < 3°$	Σ3 $\Delta\theta = 3 - 8.66°$			
A1	25	96	68	18	10	4	2.0×10^{-2}	10.7	142
A2	28	97	72	17	7	4	1.5×10^{-2}	10.3	142

the EBSD maps analyzed in our work a distinction was made between Σ3 boundaries characterized by either $\Delta\theta < 3°$ or $\Delta\theta = 3 - 8.66°$ (see Fig. 4). The former included predominantly true twin boundaries and a small number of non-twin Σ3 boundaries with misorientations close to the exact 60° ⟨1 1 1⟩ relationship.

Inspection of the surface revealed grooves at grain boundaries (see Fig. 5a). The smallest average values of the groove depth were recorded for coherent twin boundaries (CTBs), followed by low angle ($\theta < 10°$) boundaries (see Fig. 6a). Boundaries with misorientations greater than 10°, incoherent twin boundary (ITB) segments and non-twin (NT) Σ3 boundaries had deeper grooves than the former two boundary types. A similar correlation was observed between the boundary type and angles characterizing inclinations of groove walls (Fig. 6b). The mean surface roughness S_A in the A1 condition was 10.7 nm (Table 1).

3.2. Additionally annealed condition A2

During additional annealing at 1025 °C for 1 h the average grain size increased from 25 to 28 μm, without affecting the hardness of the material (see Table 1). Grain growth was accompanied by a slight increase both in the area fraction of the cube texture and in the fraction of LAGBs (Fig. 3 and Table 1). To evaluate the overall change in the boundary network due to both the increased average grain size and reduced fraction of low angle boundaries, we considered the length of boundary traces per unit area L_A [24,25], taking into account all boundary types with misorientations above 10°. The $L_{A(\theta>10°)}$ values derived from the EBSD data were corrected for a stepped nature of inclined boundary traces in the EBSD maps [24]. It was found that $L_{A(\theta>10°)}$ decreased after the additional annealing from 2.0×10^{-2} to 1.5×10^{-2} μm^{-1} (see Table 1).

By inspecting the same regions in the A1 and A2 conditions it was possible to identify which boundaries migrated during the additional annealing and which boundaries did not change their surface positions (see Fig. 5). In the current study, these two groups of boundaries are referred to as migrating and stationary boundaries, respectively. No distinction between stationary and migrating boundaries was made for ITB segments because these segments were typically too short to determine unambiguously whether their positions had changed during the annealing.

GB grooves were analyzed at 48 stationary boundaries and 24 migrating boundaries before and after the additional annealing (see Fig. 7). Comparing the depths of individual grooves in the two conditions, it is evident that for the majority of stationary boundaries the groove depth increased during the additional annealing (see Figs. 7 and 8), where the greatest changes were seen for NT Σ3 boundaries (Fig. 8a). In contrast to the stationary boundaries, the migrating boundaries typically developed shallower grooves in the new positions (see Figs. 7 and 8). These changes are also reflected in the average values for the different boundary types (Fig. 9).

The migrating boundaries not only formed new GB grooves, but also left grooves in their previous positions (Fig. 5). On average, the depth of these abandoned grooves was ~25% less than the depth of the corresponding GB grooves in the A1 condition. The mean surface roughness was measured to be 10.3 nm in the A2 condition (Table 1).

4. Discussion

The present experiment demonstrates that annealing of a recrystallized Ni–5at.%W sample at 1025 °C for 1 h changes the

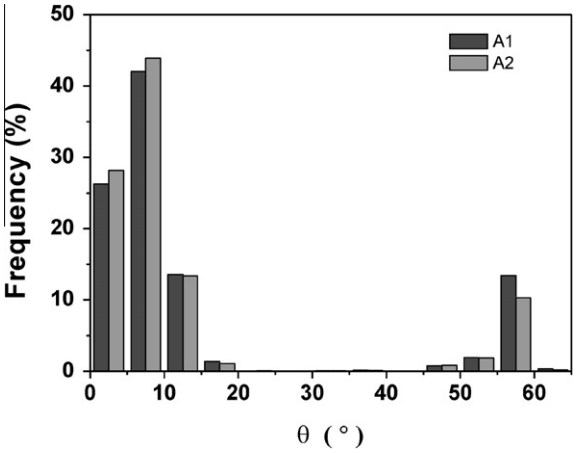

Fig. 3. Distribution of misorientation angles in the A1 and A2 conditions.

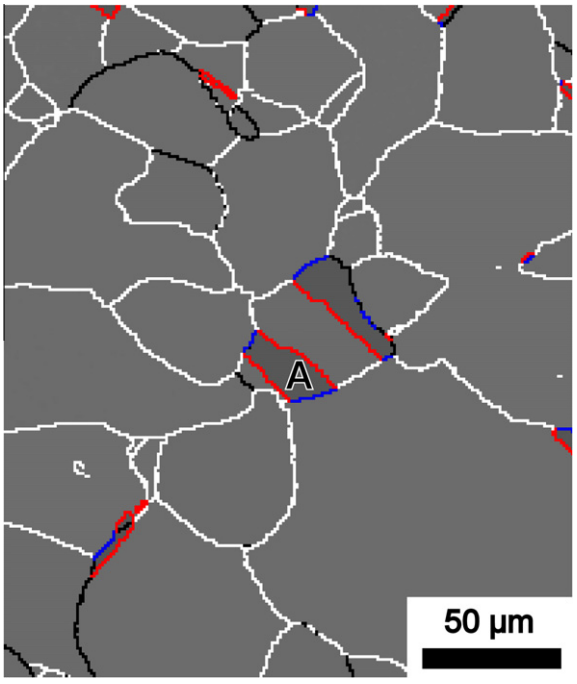

Fig. 4. A boundary map representing the microstructure in the A1 condition. In this map, 1.5–10° misorientations are shown by white lines. Boundaries with misorientations $\theta > 10°$ (except Σ3) are depicted by black lines. Σ3 boundaries characterized by small ($\Delta\theta < 3°$) and large ($\Delta\theta = 3 - 8.66°$) deviations from the exact twin relationship are shown in red and blue, respectively. The letter A is a reference label (see also Fig. 5). (For interpretation of the references to color in this figure legend, the reader is referred to the web version of this article.)

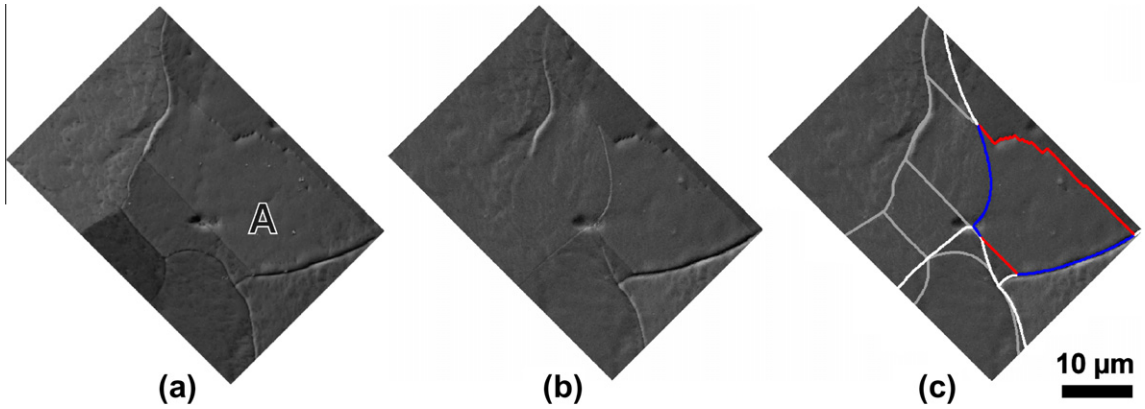

Fig. 5. SEM micrographs and a sketch illustrating different boundary types from a region in the center of Fig. 4, where the microstructure was analyzed before and after the additional annealing: (a) condition A1; (b,c) condition A2. In (c) superimposed lines indicate different boundary types. Low angle ($\theta < 10°$) boundaries, true twin boundaries and non-twin Σ3 boundaries are shown by white, red and blue lines, respectively. Gray lines indicate positions of grain boundaries before the additional annealing. The abandoned grooves in these positions can be distinguished in (b). The letter A is a reference label (see also Fig. 4). (For interpretation of the references to color in this figure legend, the reader is referred to the web version of this article.)

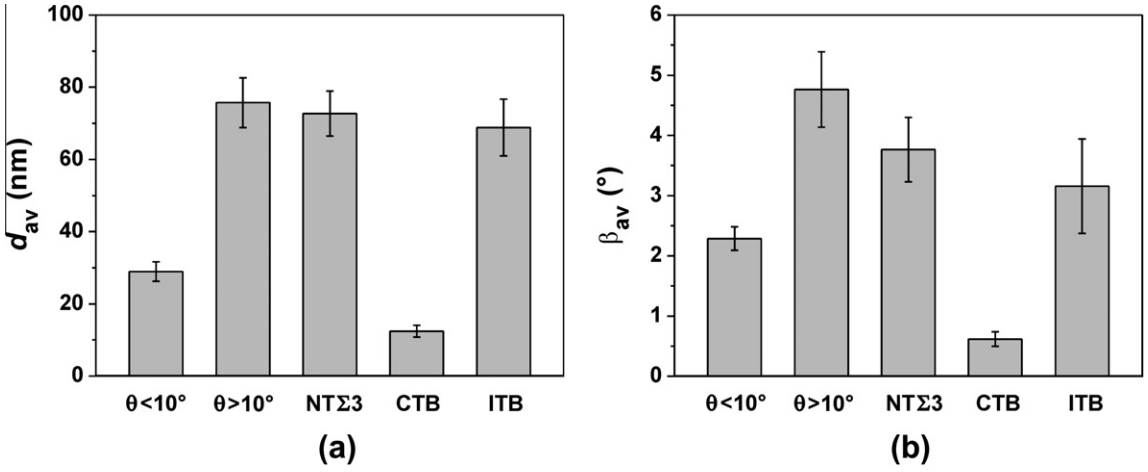

Fig. 6. Average parameters of GB grooves at different boundary types in the A1 condition: (a) depths d_{av}; (b) inclination angles β_{av} (see Fig. 1). Note that the group "$\theta > 10°$" does not include any Σ3 boundaries. The error bars correspond to the standard error.

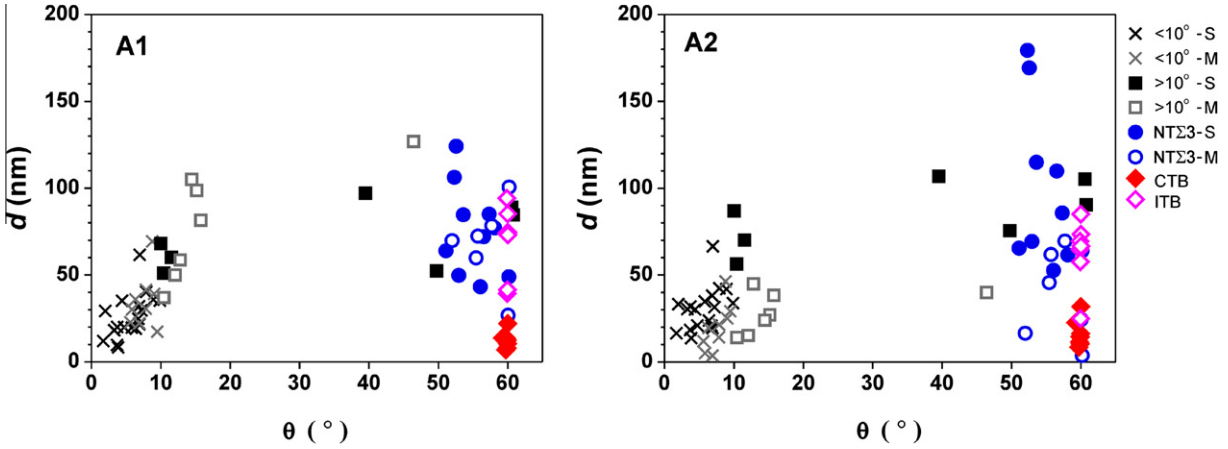

Fig. 7. Groove depths for different boundaries analyzed in the same regions of the A1 and A2 conditions. Letters "S" and "M" correspond to stationary and migrating boundaries, respectively. No distinction between stationary and migrating boundaries is made for ITBs.

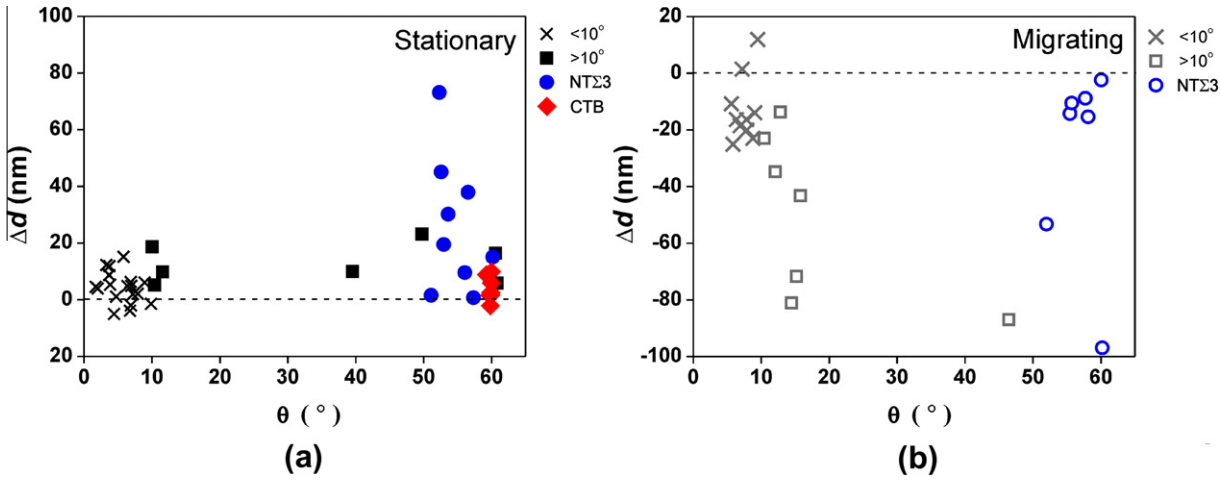

Fig. 8. The difference between depths of individual grooves at stationary (a) and migrating (b) boundaries in the A1 and A2 conditions ($\Delta d = d_{A2} - d_{A1}$).

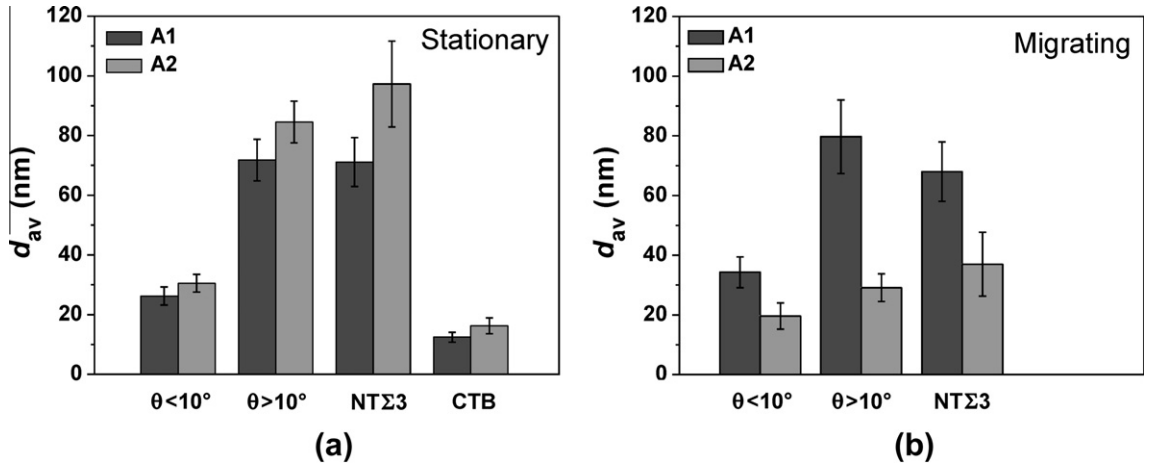

Fig. 9. Mean values of GB groove depths for stationary (a) and migrating (b) boundaries of different types. The group "$\theta > 10°$" does not include any Σ3 boundaries. The error bars correspond to the standard error.

microstructure, texture and topography of the sample. These changes are considered in the following.

4.1. Evolution of texture and grain boundary network

A strong cube texture is frequently formed during recrystallization of heavily rolled face centered cubic materials such as, for example, copper, nickel and aluminum. In the present work, the cube texture occupied approximately 96% of the total area of the Ni–5at.%W sample in the A1 condition. This is slightly lower than the fractions reported for the same alloy by Eickemeyer et al. [3,6], but similar to the values obtained by Chen et al. [26]. It should be noted that, in contrast to the substrates developed by Eickemeyer et al. [3,6], who applied either an extremely large (99.6%) total reduction or an intermediate annealing treatment in their processing schedule, the very strong texture was produced in the present work after a smaller total reduction and with no intermediate annealing.

In agreement with many previous reports, most boundary misorientations in our strongly textured material were very low. A significant fraction of boundaries with misorientations greater than 10° was however still present in the A1 condition. Interestingly, despite a very low intensity of the {2 1 2}⟨1 2 2⟩ component in this material (Fig. 2), Σ3 boundaries comprised a substantial fraction of the boundary network (Table 1). Apparently, this is due to the morphology of annealing twins seen in the microstructure. The twins are usually very narrow, but extended and contain multiple steps (facets) along twin boundaries, resulting in a significant total fraction of Σ3 boundaries in the EBSD maps.

While migration of boundaries with very low misorientations is restricted, boundaries with sufficiently large misorientations (except for coherent twin boundaries) can migrate over significant distances (see Fig. 5b), thus increasing the average grain size during further annealing at 1025 °C. During this process, grains oriented differently from the cube texture tend to shrink, increasing the fraction of the cube texture component, and new low angle boundaries are formed. The process of grain growth in the presence of the strong texture reduces the initial $L_{A(\theta>10°)}$ value by 25% (see Table 1). This suggests that an additional heat-treatment at 1025 °C of the investigated Ni–5at.%W substrate would not have a detrimental effect on the texture and boundary network in the final superconducting tape. On the contrary, as the microstructure coarsens and the fraction of low angle boundaries increases, the surface area of boundaries able to reduce the critical current density in the superconducting layer is expected to decrease compared to that in the initial condition.

4.2. Topographic changes

It is known that GB grooving may increase the overall surface roughness of Ni-based substrates [27]. Since the extent of GB grooving is sensitive to the boundary structure, special attention in this work was paid to the analysis of grooves at different boundary types. As expected, very shallow grooves were observed at low-energy LAGBs, in agreement with the data for cube-textured Ni and Ni–Cr substrates [28]. For these materials, Gladstone et al. [28] also reported a wide range of groove depths for Σ3 boundaries, which was attributed to mixing coherent and incoherent segments in their data set. This bias is avoided in the present experiment, where grooves at coherent and incoherent twin segments are analyzed separately along with a separate analysis of non-twin Σ3 boundaries. It is shown that grooves at both incoherent twin and non-twin Σ3 boundaries are typically much deeper than those at coherent interfaces, which reflects their different energies [29]. In fact, the d_{av} and β_{av} values for grooves at the former two boundary types approached the corresponding values for grooves at general boundaries with misorientation angles greater than 10° (see Fig. 6). It is therefore evident that for establishing a correlation between the boundary type and the extent of grooving, it is not sufficient to identify the boundary type solely based upon Brandon's criterion. The boundary plane and the presence of non-twin Σ3 boundaries should be taken into account to obtain an appropriate description of such correlations.

Furthermore, by separating stationary and migrating boundaries we were able to describe the changes in groove depth for these two groups of boundaries. We observed that for the majority of stationary boundaries the depth of grooves increased due to the higher temperature of the additional annealing. For a small number of boundaries in this group, the groove depth was found to decrease slightly (by 1–5 nm, see Fig. 8a). The reason for this unexpected reduction is not very clear at present. One possible explanation is that this reduction is due to the fact that locations, where groove profiles were analyzed across individual boundaries, were not absolutely identical.

Most of the migrating boundaries did not have enough time to develop deep grooves in their new positions and therefore became shallower after the additional annealing (see Fig. 8(b)). The average groove depths for the migrating boundaries were therefore much less compared to those before the additional annealing (Fig. 9b). The abandoned grooves observed behind the migrating boundaries (Fig. 5) also become shallower due to a healing process described by Mullins [14]. In our experiment, this process resulted in a 25% reduction in the average depth of the abandoned grooves.

Despite the changes observed in the extent of grooving, the mean surface roughness was almost unchanged (Table 1). This suggests that for the given heat-treatment the roughening effects due to increased grooving at some boundaries and due to appearance of new GB grooves were effectively counterbalanced by diffusional smoothing of the intragranular surface [27].

5. Conclusions

Microstructure, texture and topography have been studied in a strongly textured Ni–5at.%W substrate in the initial recrystallized condition and after additional annealing at 1025 °C for 1 h. The following conclusions were drawn.

1. A strong correlation between the average depth of grain boundary grooves and boundary type was observed in the initial condition. The smallest average groove depth was recorded for coherent twin boundaries, followed by low angle (<10°) grain boundaries. Significantly greater average GB groove depths were found for other boundary types. A similar correlation was also observed between the boundary type and the average inclination angle of groove walls.
2. The additional annealing resulted in a slight increase in the average grain size, texture strengthening and, as a result of this, an increased fraction of low angle grain boundaries. The total length of boundary traces with misorientations greater than 10° decreased by 25% as evaluated from the EBSD data.
3. During the additional annealing some boundaries did not move from their original positions, while other boundaries migrated. For the majority of stationary boundaries the groove depth increased compared to the values recorded before the additional annealing. In contrast, the migrating boundaries typically developed shallower GB grooves than those in the initial condition. The migrating boundaries also left grooves behind in the interior of the coarsened grains. The average depth of these abandoned grooves was ~25% less than the depth of the same grooves at grain boundaries before migration. The mean surface roughness was however almost unchanged.

Acknowledgements

This work was supported by the Danish Ministry of Science, Technology and Innovation under contract number 09-065234. The authors gratefully acknowledge Dr. Y. Zhao and Mr. O. Trinhammer for valuable discussions of AFM measurements.

References

[1] A. Goyal, D.P. Norton, J.D. Budai, M. Paranthaman, E.D. Specht, D.M. Kroeger, D.K. Christen, Q. He, B. Saffian, F.A. List, D.F. Lee, P.M. Martin, C.E. Klabunde, E. Hatfield, V.K. Sikka, Appl. Phys. Lett. 69 (1795) (1996) 1795–1797.
[2] J. Eickemeyer, D. Selbmann, R. Opitz, B. De Boer, B. Holzapfel, L. Schultz, U. Miller, Supercond. Sci. Technol. 14 (2001) 152–159.
[3] J. Eickemeyer, D. Selbmann, R. Opitz, H. Wendrock, E. Maher, U. Miller, W. Prusseit, Phys. C 372–376 (2002) 814–817.
[4] B. de Boer, J. Eickemeyer, N. Reger, L. Fernandez, J. Richter, B. Holzapfel, L. Schultz, W. Prusseit, P. Berberich, Acta Mater. 49 (2001) 1421–1428.
[5] S. Engel, K. Knoth, R. Hühne, L. Schultz, B. Holzapfel, Supercond. Sci. Technol. 18 (2005) 1385–1390.
[6] J. Eickemeyer, R. Hühne, A. Güth, C. Rodig, H. Klauß, B. Holzapfel, Supercond. Sci. Technol. 21 (2008) 105012.
[7] J.H. Durrell, N.A. Rutter, Supercond. Sci. Technol. 22 (2009) 013001.
[8] E. Varesi, G. Celentano, T. Petrisor, V. Boffa, L. Ciontea, V. Galluzzi, U. Gambardella, A. Mancini, A. Rufoloni, A. Vannozzi, Supercond. Sci. Technol. 16 (2003) 498–505.
[9] U. Schoop, M.W. Rupich, C. Thieme, D.T. Verebelyi, W. Zhang, X. Li, T. Kodenkandath, N. Nguyen, E. Siegal, L. Civale, T. Holesinger, B. Maiorov, A. Goyal, M. Paranthaman, IEEE Trans. Appl. Supercond. 15 (2005) 2611–2616.
[10] M.P. Paranthaman, X. Qiu, F.A. List, K. Kim, Y. Zhang, X. Li, S. Sathyamurthy, C. Thieme, M.W. Rupich, IEEE Trans. Appl. Supercond. 21 (2011) 3059–3061.
[11] R.I. Tomov, A. Kursumovic, M. Majoros, B.A. Glowacki, J.E. Evetts, A. Tuissi, E. Villa, M. Zamboni, Y. Sun, S. Tönies, H.W. Weber, Phys. C 383 (2003) 323–336.
[12] A.C. Wulff, Y. Zhao, O.V. Mishin, J.-C. Grivel, J. Supercond. Nov. Magn. 25 (2012) 475–479.
[13] K. Knoth, R. Hühne, S. Oswald, L. Schultz, B. Holzapfel, Acta Mater. 55 (2007) 517–529.
[14] W.W. Mullins, Acta Metal. 6 (1958) 414–427.
[15] Y. Zhao, J.-C. Grivel, A.B. Abrahamsen, D. Pavlopoulos, J. Bednarcik, M. von Zimmermann, IEEE Trans. Appl. Supercond. 21 (2011) 2912–2915.
[16] A.C. Wulff, O.V. Mishin, J.-C. Grivel, Phys. Procedia (2012), http://dx.doi.org/10.1016/j.phpro.2012.06.147.
[17] S. Sathyamurthy, M. Paranthaman, T. Aytug, B.W. Kang, P.M. Martin, A. Goyal, D.M. Kroeger, D.K. Christen, J. Mater. Res. 17 (2002) 1543–1549.
[18] M.S. Bhuiyan, M. Paranthaman, S. Sathyamurthy, T. Aytug, S. Kang, D.F. Lee, A. Goyal, E.A. Payzant, K. Salama, Supercond. Sci. Technol. 16 (2003) 1305–1309.
[19] D.A. Bonnell, B.D. Huey, in: D.A. Bonnell (Ed.), Scanning Probe Microscopy and Spectroscopy, 2nd edn., Wiley, New York, 2001, pp. 32–42.
[20] D.M. Saylor, G.S. Rohrer, J. Am. Ceram. 82 (1999) 1529–1536.
[21] O.V. Mishin, X. Huang, Mater. Sci. Forum 294–296 (1999) 401–404.
[22] O.V. Mishin, J. Mater. Sci. 33 (1998) 5137–5143.
[23] D.C. Brandon, Acta Metall. 14 (1966) 1479–1484.
[24] W.Q. Cao, A. Godfrey, Q. Liu, Mater. Sci. Eng., A 361 (2003) 9–14.
[25] O.V. Mishin, V.M. Segal, S. Ferrasse, Metal. Mater. Trans. A (2012), http://dx.doi.org/10.1007/s11661-012-1287-1.

[26] S.K. Chen, C.F. Liu, P.X. Zhang, L. Zhou, Mat. Sci. Forum 546–549 (2007) 1997–2002.
[27] T.G. Truchan, F.H. Rountree, M.T. Lanagan, S.M. McClelian, D.J. Miller, K.C. Goretta, M. Tamsic, R. Foley, IEEE Trans. Appl. Supercond. 10 (2000) 1130–1133.
[28] T.A. Gladstone, J.C. Moore, A.J. Wilkinson, C.R.M. Grovenor, IEEE Trans. Appl. Supercond. 11 (2001) 2923–2926.
[29] L.E. Murr, Interfacial phenomena in metals and alloys, Addison-Wesley Pub. Co., Reading, MA, 1975.